

USB: Universal-Scale Object Detection Benchmark

Yosuke Shinya*



Figure 1. Universal-scale object detection. For realizing human-level perception, object detection systems must detect both tiny and large objects, even if they are out of natural image domains. To this end, we introduce the *Universal-Scale object detection Benchmark (USB)* that consists of the COCO dataset (left), Waymo Open Dataset (middle), and Manga109-s dataset (right).

Abstract

Benchmarks, such as COCO, play a crucial role in object detection. However, existing benchmarks are insufficient in scale variation, and their protocols are inadequate for fair comparison. In this paper, we introduce the *Universal-Scale object detection Benchmark (USB)*. USB has variations in object scales and image domains by incorporating COCO with the recently proposed Waymo Open Dataset and Manga109-s dataset. To enable fair comparison and inclusive research, we propose training and evaluation protocols. They have multiple divisions for training epochs and evaluation image resolutions, like weight classes in sports, and compatibility across training protocols, like the backward compatibility of the Universal Serial Bus. Specifically, we request participants to report results with not only higher protocols (longer training) but also lower protocols (shorter training). Using the proposed benchmark and protocols, we analyzed eight methods and found weaknesses of existing COCO-biased methods. The code is available at <https://github.com/shinya7y/UniverseNet>.

1. Introduction

Humans can detect various objects. See Figure 1. One can detect close equipment in everyday scenes, far vehicles in traffic scenes, and texts and persons in manga (Japanese

comics). If computers can automatically detect various objects, they will yield significant benefits to humans. For example, they will help impaired people and the elderly, save lives by autonomous driving, and provide safe entertainment during pandemics by automatic translation.

Researchers have pushed the limits of object detection systems by establishing datasets and benchmarks [41]. One of the most important milestones is PASCAL VOC [19]. It has enabled considerable research on object detection, leading to the success of deep learning-based methods and successor datasets such as ImageNet [55] and COCO [40]. Currently, COCO serves as the standard dataset and benchmark for object detection because it has several advantages over PASCAL VOC [19]. COCO contains more images, categories, and objects (especially small objects) in their natural context [40]. Using COCO, researchers can develop and evaluate methods for multi-scale object detection. However, the current object detection benchmarks, especially COCO, have the following two problems.

Problem 1: Variations in object scales and image domains remain limited. To realize human-level perception, computers must handle various object scales and image domains as humans can. Among various domains [70], the traffic and artificial domains have extensive scale variations (see Sec. 3). COCO is far from covering them. Nevertheless, the current computer vision community is overconfident in COCO results. For example, most studies on state-of-the-art methods in 2020 only report COCO results [13, 14, 34, 36, 71, 76] or those for bounding box ob-

*This work was done independently of the author's employer.

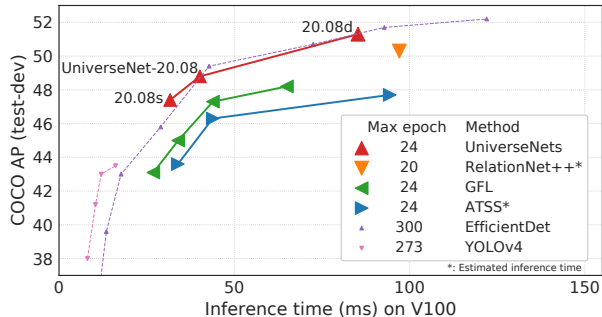


Figure 2. Speed-accuracy trade-offs in the current standard COCO benchmark. Most studies train models with standard settings (e.g., within 24 epochs), while some studies train with abnormal settings (e.g., 300 epochs). For fair comparison, we propose *USB protocols* that urge the latter studies to report results with standard settings.

ject detection [5, 18, 51, 66]. Readers cannot assess whether these methods are specialized for COCO or generalizable to other datasets and domains.

Problem 2: Protocols for training and evaluation are not well established. There are standard experimental settings for the COCO benchmark [11, 24, 36, 38, 39, 68, 76]. Many studies train detectors within 24 epochs using a learning rate of 0.01 or 0.02 and evaluate them on images within 1333×800 . These settings are not obligations but non-binding agreements for fair comparison. Some studies do not follow the settings for accurate and fast detectors¹. Their abnormal and scattered settings hinder the assessment of the most suitable method (see Figure 2). Furthermore, by “buying stronger results” [56], they build a barrier for those without considerable funds to develop and train detectors.

This study makes the following two contributions to resolve the problems.

Contribution 1: We introduce the *Universal-Scale object detection Benchmark (USB)* that consists of three datasets. In addition to COCO, we selected the Waymo Open Dataset [61] and Manga109-s [3, 45] to cover various object scales and image domains. They are the largest public datasets in their domains and enable reliable comparisons. To the best of our knowledge, USB is the first benchmark beyond COCO that evaluates finer scale-wise metrics across multiple domains. We conducted experiments using eight methods and found weaknesses of existing COCO-biased methods.

Contribution 2: We established the *USB protocols* for fair training and evaluation, inspired by weight classes in sports and the backward compatibility of the Universal Serial Bus. Specifically, USB protocols enable fair and easy comparisons by defining multiple divisions for train-

¹YOLOv4 was trained for 273 epochs [5], DETR for 500 epochs [10], EfficientDet-D6 for 300 epochs [66], and EfficientDet-D7x for 600 epochs [67]. SpineNet uses a learning rate of 0.28 [18], and YOLOv4 uses a searched learning rate of 0.00261 [5]. EfficientDet finely changes the image resolution from 512×512 to 1536×1536 [66].

ing epochs and evaluation image resolutions. Furthermore, we introduce compatibility across training protocols by requesting participants to report results with not only higher protocols (longer training) but also lower protocols (shorter training). To the best of our knowledge, our training protocols are the first ones that allow for both fair comparisons with shorter training and strong results with longer training. Our protocols promote inclusive, healthy, and sustainable object detection research.

2. Related Work

2.1. Object Detection Methods

Deep learning-based detectors dominate the recent progress in object detection [41]. They can be divided [11, 41, 53] as single-stage detectors without region proposal [39, 42, 52] and multi-stage (including two-stage) detectors with region proposal [9, 38, 53]. Detecting multi-scale objects is a fundamental challenge in object detection [8, 41]. Various components have been improved, including backbones and modules [15, 21, 28, 29, 62], necks [38, 66, 71], heads and training sample selection [42, 53, 76], and multi-scale training and testing [54, 59, 76] (see Supplementary Material for the details of related work). Unlike most prior studies, we analyzed their methods across various object scales and image domains through the proposed benchmark.

2.2. Object Detection Benchmarks

There are numerous object detection benchmarks. For specific (category) object detection, recent benchmarks such as WIDER FACE [74] and TinyPerson [75] contain tiny objects. Although they are useful for evaluation for a specific category, many applications should detect multiple categories. For autonomous driving, KITTI [22] and Waymo Open Dataset [61] mainly evaluate three categories (car, pedestrian, and cyclist) in their leaderboards. For generic object detection, PASCAL VOC [19] and COCO [40] include 20 and 80 categories, respectively. The number of categories has been further expanded by recent benchmarks, such as Open Images [35], Objects365 [57], and LVIS [26]. All the above datasets comprise photographs, whereas Clipart1k, Watercolor2k, Comic2k [33], and Manga109-s [3, 45] comprise artificial images. Although Waymo Open Dataset [61] and Manga109-s [3, 45] have extensive scale variations (see Sec. 3.3), scale-wise metrics have not been evaluated [49, 61].

Detectors evaluated on a specific dataset may perform worse on other datasets or domains. To address this issue, some benchmarks consist of multiple datasets. In the Robust Vision Challenge 2020 [1], detectors were evaluated on three datasets in the natural and traffic image domains. For *universal-domain* object detection, the Universal Object

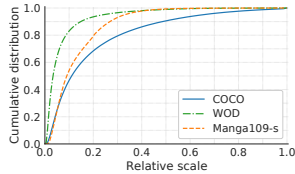


Figure 3. Object scale distributions based on relative scale [32, 59, 75]. USB covers extensive scale variations quantitatively.

Detection Benchmark (UODB) [70] comprises 11 datasets in the natural, traffic, aerial, medical, and artificial image domains. Although it is suitable for evaluating detectors in various domains, variations in object scales are limited. Unlike UODB, our USB focuses on *universal-scale* object detection. The datasets in USB contain more instances, including tiny objects, than the datasets used in UODB.

As discussed in Sec. 1, the current benchmarks allow extremely unfair settings (e.g., $25\times$ training epochs). We resolved this problem by establishing USB protocols for fair training and evaluation.

3. Benchmark Protocols of USB

Here, we present the principle, datasets, protocols, and metrics of USB. See Supplementary Material for additional information.

3.1. Principle

We focus on the *Universal-Scale Object Detection (USOD)* task that aims to detect various objects in terms of object scales and image domains. Unlike separate discussions for multi-scale object detection (Sec. 2) and universal (-domain) object detection [70], USOD does not ignore the relation between scales and domains (Sec. 3.3).

For various applications and users, benchmark protocols should cover from short to long training and from small to large test scales. On the other hand, they should not be scattered for meaningful benchmarks. To satisfy the conflicting requirements, we define multiple divisions for training epochs and evaluation image resolutions. Furthermore, we urge participants who have access to extensive computational resources to report results with standard training settings. This request enables fair comparison and allows many people to develop and compare object detectors.

3.2. Definitions of Object Scales

Following the TinyPerson benchmark [75], we consider two types of object scales. The absolute scale is calculated as \sqrt{wh} , where w and h denote the object’s width and height, respectively. The relative scale is calculated as $\sqrt{\frac{wh}{WH}}$, where W and H denote the image’s width and height, respectively.

Dataset	Domain	Color	Main sources of scale variation
COCO [40]	Natural	RGB	Categories, distance
WOD [61]	Traffic	RGB	Distance
Manga109-s [3, 45]	Artificial	Grayscale*	Viewpoints, page layouts

Table 1. Characteristics of datasets. USB covers many qualitative variations related to scales and domains. *: Few RGB images.

Benchmark	Dataset	Boxes	Images	B/I	Scale variation [†]
USB (Ours)	COCO [40]	897 k (3.1 \times)	123 k	7.3	88.8 (1.0 \times)
	WOD [61] v1.2 f0	1.0 M (29 \times)	100 k	10.0	96.7 (5.8 \times)
	Manga109-s [3, 45]	401 k (63 \times)	8.2 k	49.2	28.6 (1.5 \times)
UODB [70]	COCO [40] val2014	292k	41 k	7.2	89.6
	KITTI [22]	35 k	7.5 k	4.7	16.6
	Comic2k [33]	6.4k	2.0 k	3.2	19.1

Table 2. Statistics of datasets in USB and counterpart datasets in UODB [70]. Values are based on publicly available annotations. B/I: Average number of boxes per image. †: Calculated by the ratio of the 99 percentile to 1 percentile of relative scale.

3.3. Datasets

To establish USB, we selected the COCO [40], Waymo Open Dataset (WOD) [61], and Manga109-s (M109s) [3, 45]. WOD and M109s are the largest public datasets with many small objects in the traffic and artificial domains, respectively. Object scales in these domains vary significantly with distance and viewpoints, unlike those in the medical and aerial domains². USB covers extensive scale variations quantitatively (Figure 3) and qualitatively (Table 1). As shown in Table 2, these datasets contain more instances and larger scale variations than their counterpart datasets in UODB [70] (COCO [40] val2014, KITTI [22], and Comic2k [33]). USOD needs to evaluate detectors on datasets with many instances because more instances enable more reliable comparisons of scale-wise metrics.

For the first dataset, we adopted the COCO dataset [40]. COCO contains natural images of everyday scenes collected from the Internet. Annotations for 80 categories are used in the benchmark. As shown in Figure 1 (left), object scales mainly depend on the categories and distance. Although COCO contains objects smaller than those of PASCAL VOC [19], objects in everyday scenes (especially indoor scenes) are relatively large. Since COCO is the current standard dataset for multi-scale object detection, we adopted the same training split `train2017` (also known as `trainval35k`) as the COCO benchmark to eliminate the need for retraining across benchmarks. We adopted the `val2017` split (also known as `minival`) as the test set.

For the second dataset, we adopted the WOD, which is a large-scale, diverse dataset for autonomous driving [61] with many annotations for tiny objects (Figure 3). The images were recorded using five high-resolution cameras

²Aerial datasets contain abundant small objects but scarce large ones (see Table 4 in [16]). WOD has larger scale variation by distance variation, where 1% of objects are larger than 1/4 of the image area.

Protocol	Fair	Suitable for each model	Strong results	Selectable divisions	Comparable across divisions
A) Standard (short) training	✓				
B) Lawless (no regulations)		✓	✓		
C) Ours w/o compatibility	✓	✓	✓	✓	
D) Ours	✓	✓	✓	✓	✓

Table 3. Comparison of training protocols.

mounted on vehicles. As shown in Figure 1 (middle), object scales vary mainly with distance. The full data splits of WOD are too large for benchmarking methods. Thus, we extracted 10% size subsets from the predefined training split (798 sequences) and validation split (202 sequences) [61]. Specifically, we extracted splits based on the ones place of the frame index (frames 0, 10, ..., 190) in each sequence. We call the subsets $f_{0\text{train}}$ and $f_{0\text{val}}$ splits. Each sequence in the splits contains ~ 20 frames (20 s, 1 Hz), and each frame contains five images for five cameras. We used three categories (vehicle, pedestrian, and cyclist) following the official *ALL_NS* setting [2] used in WOD competitions.

For the third dataset, we adopted the M109s [3, 45]. M109s contains artificial images of manga (Japanese comics) and annotations for four categories (body, face, frame, and text). Many characteristics differ from those of natural images. Most images are grayscale. The objects are highly overlapped [49]. As shown in Figure 1 (right), object scales vary unrestrictedly with viewpoints and page layouts. Small objects differ greatly from downsampled versions of large objects because small objects are drawn with simple lines and points. For example, small faces look like a sign (·). This characteristic may ruin techniques developed mainly for natural images. Another challenge is ambiguity in annotations. Sometimes, a small-scale object is annotated, and sometimes, a similar scale object on another page is not annotated. Since annotating small objects is difficult and labor-intensive, this is an important and practical challenge. We carefully selected 68, 4, and 15 volumes for training, validation, and testing splits, and we call them the 68train , 4val , and 15test , respectively.

We selected the test splits from images with publicly available annotations to reduce labor for submissions. Participants should not fine-tune hyperparameters based on the test splits to prevent overfitting.

3.4. Motivation of Training Protocols

We describe the motivation of our training protocols with Table 3, which compares existing protocols (A and B) and novel protocols (C and D). Protocol A is the current standard training protocol within 24 epochs, popularized by successive detectors, Detectron [24], and MMDetection [11]. This protocol is fair but not suitable for slowly convergent models (e.g., DETR [10]). Protocol B is lawless without any regulations. Participants can train their models with arbitrary settings suitable for them, even if they are

Protocol	Max epoch	AHPO	Compatibility	Example
USB 1.0	24	✗	—	2× schedule [24, 27]
USB 2.0	73	✗	USB 1.0	6× schedule [27]
USB 3.0	300	✗	USB 1.0, 2.0	EfficientDet-D6 [66]
USB 3.1	300	✓	USB 1.0, 2.0, 3.0	YOLOv4 [5]
Freestyle	∞	✓	—	EfficientDet-D7x [67]

Table 4. USB training protocols. AHPO: Aggressive hyperparameter optimization.

unfair settings (e.g., standard training for existing methods and longer training for proposed ones). Since object detectors can achieve high accuracy with long training schedules and strong data augmentation [18, 23, 67], participants can buy stronger results [56].

Both existing protocols A and B have advantages and disadvantages. Neither is appropriate. Thus, we considered novel protocols to bridge them. We first defined multiple divisions for training epochs, inspired by weight classes in sports. This Protocol C enables fair comparison in each division. Participants can select divisions according to their purposes and resources. However, we cannot compare models across divisions. To resolve this, we then came up with an idea: introducing backward compatibility like the Universal Serial Bus, resulting in Protocol D. As described above, *our protocols introduce a completely different paradigm from existing limited or unfair protocols*. To the best of our knowledge, *our protocols are the first ones that satisfy the five requirements in Table 3*.

3.5. Training Protocols

For fair training, we propose the *USB training protocols* shown in Table 4. By analogy with the backward compatibility of the Universal Serial Bus³, USB training protocols emphasize compatibility between protocols. Importantly, *participants should report results with not only higher protocols but also lower protocols*. For example, when a participant trains a model for 150 epochs with standard hyperparameters, it corresponds to USB 3.0. The participant should also report the results of models trained for 24 and 73 epochs in a paper. This reveals the effectiveness of the method by ablating the effect of long training. The readers of the paper can judge whether the method is useful for standard training epochs. Since many researchers and practitioners do not have access to extensive computational resources, such information is important to select methods.

The number of maximum epochs for USB 1.0 is 24, which is the most popular setting in COCO (Table 12). We adopted 73 epochs for USB 2.0, where models trained from scratch can catch up with those trained from ImageNet pre-trained models [27]. This serves as a guideline for comparison between models with and without pre-training, although perfectly fair comparisons are impossible considering large

³Higher protocols can adapt the data transfer rate to lower protocols.

differences caused by pre-training [58]. We adopted 300 epochs for USB 3.x such that YOLOv4 [5] and most EfficientDet models [67] correspond to this protocol. Models trained for more than 300 epochs are regarded as Freestyle. They are not suitable for benchmarking methods, although they may push the empirical limits of detectors [10, 67]. The correspondences between Tables 3 and 4 are as follows: Protocol A corresponds to only USB 1.0; Protocol B corresponds to only Freestyle; Protocol C corresponds to all protocols (divisions) in Table 4 without compatibility; and Protocol D corresponds to all protocols (divisions) in Table 4 with compatibility.

For models trained with annotations other than 2D bounding boxes (*e.g.*, instance/stuff/panoptic segmentation, keypoint, caption, and point cloud), 0.5 is added to their number of protocols. Participants should also report results without such annotations if possible for their algorithms.

For ease of comparison, we limit the pre-training datasets to the three datasets and ImageNet-1k (ILSVRC 1,000-class classification) [55]. Other datasets are welcome only when the results with and without additional datasets are reported. Participants should describe how to use the datasets. A possible way is to fine-tune models on WOD and M109s from COCO pre-trained models. Another way is to train a single model jointly [70] on the three datasets.

In addition to long training schedules, hyperparameter optimization is resource-intensive. If authors of a paper fine-tune hyperparameters for their architecture, other people without sufficient computational resources cannot compare methods fairly. For hyperparameters that need to be tuned exponentially, such as learning rates and $1 - m$ where m denotes momentum, the minimum ratio of hyperparameter choices should be greater than or equal to 2 (*e.g.*, choices $\{0.1, 0.2, 0.4, 0.8, \dots\}$, $\{0.1, 0.2, 0.5, 1.0, \dots\}$, and $\{0.1, 0.3, 1.0, \dots\}$). For hyperparameters that need to be tuned linearly, the number of choices should be less than or equal to 11 (*e.g.*, choices $\{0.0, 0.1, 0.2, \dots, 1.0\}$). When participants perform aggressive hyperparameter optimization (AHPO) by manual fine-tuning or automatic algorithms, 0.1 is added to their number of protocols. They should report both results with and without AHPO.

To further improve fairness without sacrificing the practicality and simplicity of the protocols, we consider it a kind of AHPO to use data augmentation techniques that more than double the time per epoch.

3.6. Evaluation Protocols

For fair evaluation, we propose the *USB evaluation protocols* shown in Table 5. By analogy with the size variations of the Universal Serial Bus connectors for various devices, USB evaluation protocols have variations in test image scales for various devices and applications.

The maximum resolution for Standard USB follows the

Protocol	Max reso.	Typical scale	Reference
Standard USB	1,066,667	1333×800	Popular in COCO [11, 24, 40]
Mini USB	262,144	512×512	Popular in VOC [19, 42]
Micro USB	50,176	224×224	Popular in ImageNet [28, 55]
Large USB	2,457,600	1920×1280	WOD front cameras [61]
Huge USB	7,526,400	3360×2240	WOD top methods ([32], ours)
Freestyle	∞	—	—

Table 5. USB evaluation protocols.

popular test scale of 1333×800 in the COCO benchmark (Table 12, [11, 24]). For Mini USB, we limit the resolution based on 512×512. This resolution is popular in the PASCAL VOC benchmark [19, 42], which contains small images and large objects. It is also popular in real-time detectors [5, 66]. We adopted a further small-scale 224×224 for Micro USB. This resolution is popular in ImageNet classification [28, 55]. Although small object detection is extremely difficult, it is suitable for low-power devices. Additionally, this protocol enables people to manage object detection tasks using one or few GPUs. To cover larger test scales than Standard USB, we define Large USB and Huge USB based on WOD resolutions (see Supplementary Material for the top methods). Although larger inputs (regarded as Freestyle) may be preferable for accuracy, excessively large inputs reduce the practicality of detectors.

In addition to test image scales, the presence and degree of Test-Time Augmentation (TTA) make large differences in accuracy and inference time. When using TTA, participants should report its details (including the number of scales of multi-scale testing) and results without TTA.

3.7. Evaluation Metrics

We mainly use the COCO metrics [37, 40] to evaluate the performance of detectors on each dataset. We provide data format converters for WOD⁴ and M109s⁵.

We first describe the calculation of COCO metrics according to the official evaluation code [37]. True or false positives are judged by measuring the Intersection over Union (IoU) between predicted bounding boxes and ground truth bounding boxes [19]. For each category, the Average Precision (AP) is calculated as precision averaged over 101 recall thresholds $\{0, 0.01, \dots, 1\}$. The COCO-style AP (CAP) for a dataset d is calculated as

$$\text{CAP}_d = \frac{1}{|T|} \sum_{t \in T} \frac{1}{|C_d|} \sum_{c \in C_d} \text{AP}_{t,c}, \quad (1)$$

where $T = \{0.5, 0.55, \dots, 0.95\}$ denotes the predefined 10 IoU thresholds, C_d denotes categories in the dataset d , $|\cdot|$ denotes the cardinality of a set (*e.g.*, $|C_d| = 80$ for COCO), and $\text{AP}_{t,c}$ denotes AP for an IoU threshold t and a category c . For detailed analysis, five additional AP metrics (averaged over categories) are evaluated. AP_{50} and AP_{75} denote

⁴<https://github.com/shinya7y/WaymoCOCO>

⁵<https://github.com/shinya7y/manga109api>

AP at single IoU thresholds of 0.5 and 0.75, respectively. AP_S , AP_M , and AP_L are variants of CAP, where target objects are limited to small (area $\leq 32^2$), medium ($32^2 \leq \text{area} \leq 96^2$), and large ($96^2 \leq \text{area}$) objects, respectively. The area is measured using mask annotations for COCO and bounding box annotations for WOD and M109s.

As the primary metric for USB, we use the mean COCO-style AP (mCAP) averaged over all datasets D as

$$\text{mCAP} = \frac{1}{|D|} \sum_{d \in D} \text{CAP}_d. \quad (2)$$

Since USB adopts the three datasets described in Sec. 3.3, $\text{mCAP} = (\text{CAP}_{\text{COCO}} + \text{CAP}_{\text{WOD}} + \text{CAP}_{\text{M109s}})/3$. Similarly, we define five metrics from AP_{50} , AP_{75} , AP_S , AP_M , and AP_L by averaging them over the datasets.

The three COCO-style scale-wise metrics (AP_S , AP_M , and AP_L) are too coarse for detailed scale-wise analysis. They confuse objects of significantly different scales. For example, the absolute scale of a large object might be 100 or 1600. Thus, we introduce finer scale-wise metrics. We define the *Absolute Scale AP (ASAP)* and *Relative Scale AP (RSAP)* using exponential thresholds. ASAP partitions object scales based on absolute scale $(0, 8, 16, 32, \dots, 1024, \infty)$. RSAP partitions object scales based on relative scale $(0, \frac{1}{256}, \frac{1}{128}, \dots, \frac{1}{2}, 1)$. We call the partitions by their maximum scales.

For ease of quantitative evaluation, we limit the number of detections per image to 100 across all categories, following the COCO benchmark [37]. For qualitative evaluation, participants may raise the limit to 300 (1% of images in the M109s 15_{test} set contain more than 100 annotations).

4. Experiments

Here, we present benchmark results and analysis on USB. Thereafter, we rethink state-of-the-art methods on COCO with the USB protocols. See Supplementary Material for the details of the experimental settings and results, including additional analysis and ablation studies.

4.1. Experimental Settings

We compared and analyzed eight methods (detectors), using ResNet-50-B [28, 29] as the default backbone. Two of them are popular multi-stage detectors: (1) Faster R-CNN [53] with FPN [38] and (2) Cascade R-CNN [9]. Three of them are popular single-stage detectors: (3) RetinaNet [39], (4) ATSS [76], and (5) GFL [36]. We designed three additional detectors for USOD by collecting methods for multi-scale object detection. (6) *ATSEPC*: ATSS [76] with SEPC without iBN [71]. (7) *UniverseNet*: ATSEPC with Res2Net-50-v1b [21], Deformable Convolutional Networks (DCN) [15], and multi-scale training. (8) *UniverseNet-20.08*: A variant of UniverseNet designed around August 2020 with GFL [36], SyncBN [50],

iBN [71], and the light use of DCN [15, 71]. See Supplementary Material for the details of the methods and architectures used in UniverseNets.

Our code is built on MMDetection [11] v2. We trained all models with Stochastic Gradient Descent (SGD). COCO models were fine-tuned from ImageNet [55] pre-trained backbones. We trained the models for WOD and M109s from the corresponding COCO pre-trained models.

Hyperparameters	COCO	WOD	M109s	Hyperparam.	Common
LR for multi-stage detectors	0.02	0.02	0.16	Epoch	12
LR for single-stage detectors	0.01	0.01	0.08	Batch size	16
Test scale	1333×800	1248×832	1216×864	Momentum	0.9
Range for multi-scale training*	480–960	640–1280	480–960	Weight decay	10^{-4}

Table 6. Default hyperparameters. *: Shorter side pixels.

The default hyperparameters are listed in Table 6. Most values follow standard settings [11, 38, 39, 76]. We used some dataset-dependent values. For M109s, we roughly tuned the learning rates (LR) based on a preliminary experiment with the RetinaNet [39] baseline model. Test scales were determined within the Standard USB protocol, considering the typical aspect ratio of the images in each dataset. We used multi-scale training for UniverseNets (see Supplementary Material for ablation results). The ranges for multi-scale training for COCO and M109s follow prior work [71]. We used larger scales for WOD because objects in WOD are especially small. We follow the learning rate schedules of MMDetection [11]. Unless otherwise specified, we used the $1 \times$ schedule (12 epochs).

4.2. Benchmark Results on USB

Main results. We trained and evaluated the methods on USB. All the methods follow the Standard USB 1.0 protocol using the default hyperparameters in Sec. 4.1. The results are shown in Table 7. UniverseNet-20.08 achieves the highest results on all the datasets, resulting in 52.1% mCAP. In most cases, methods that work on COCO also work on the other datasets. Cascade R-CNN [9] and ATSS [76] achieve over 2% more mCAP than Faster R-CNN [53] and RetinaNet [39], respectively. In some cases, however, methods that work on COCO show small or negative effects on WOD and M109s (see especially the decrease of WOD CAP from ATSS to ATSEPC). COCO-biased methods that greatly improve *only* COCO CAP do not improve mCAP much. For example, adding SEPC [71] to ATSS [76] improves mCAP by 1.0%, although it improves COCO CAP by 2.7%. Thus, USB can impose a penalty on COCO-biased methods.

Scale-wise AP. We show RSAP on USB in Figure 4. It does not increase monotonically but rather decreases at relative scales greater than $1/4$. We cannot find this weakness from the coarse COCO-style scale-wise AP in Table 7. The difficulty of very large objects may be caused by truncation or unusual viewpoints [30].

Affinity between methods and datasets. To compare the effectiveness of each method on each dataset, we show the

Method	mCAP	AP ₅₀	AP ₇₅	AP _S	AP _M	AP _L	COCO	WOD	M109s
Faster R-CNN [53]	45.9	68.2	49.1	15.2	38.9	62.5	37.4	34.5	65.8
Cascade R-CNN [9]	48.1	68.5	51.5	15.6	41.3	65.9	40.3	36.4	67.6
RetinaNet [39]	44.8	66.0	47.4	12.9	37.3	62.6	36.5	32.5	65.3
ATSS [76]	47.1	68.0	50.2	15.5	39.5	64.7	39.4	35.4	66.5
ATSEPC [71, 76]	48.1	68.5	51.2	15.5	40.5	66.8	42.1	35.0	67.1
GFL [36]	47.7	68.3	50.6	15.8	39.9	65.8	40.2	35.7	67.3
UniverseNet	51.4	72.1	55.1	18.4	45.0	70.7	46.7	38.6	68.9
UniverseNet-20.08	52.1	72.9	55.5	19.2	45.8	70.8	47.5	39.0	69.9

Table 7. Benchmark results on USB.

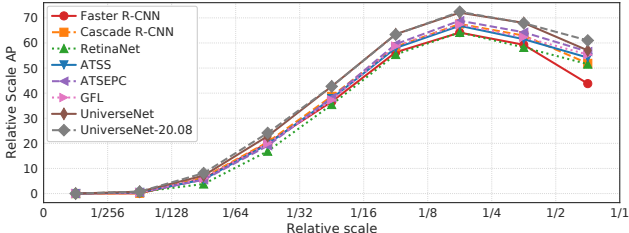


Figure 4. Relative Scale AP on USB.

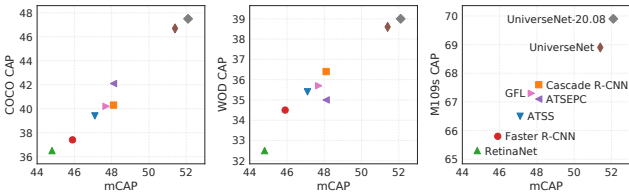


Figure 5. Correlation between mCAP and CAP on each dataset.

Backbone	mCAP	AP ₅₀	AP ₇₅	AP _S	AP _M	AP _L	COCO	WOD	M109s
ResNet-50-B [28, 29]	47.1	68.0	50.2	15.5	39.5	64.7	39.4	35.4	66.5
Swin-T [43]	49.0	70.6	52.0	17.2	41.8	67.2	43.7	37.2	66.2

Table 8. ResNet vs. Swin Transformer on USB with ATSS [76].

correlation between mCAP and CAP on each dataset in Figure 5. SEPC [71] improves COCO CAP and deteriorates WOD CAP. Multi-stage detectors [9, 53] show relatively high CAP on WOD and relatively low CAP on COCO. Adding GFL [36] is especially effective on M109s (see improvements from ATSS to GFL and from UniverseNet to UniverseNet-20.08).

Details on each dataset. Table 9 shows the COCO results. Since the effectiveness of existing methods has been verified on COCO, their improvements are steady. Table 10 shows the WOD results. AP_S on WOD is less than 10%, which is much lower than AP_S on COCO. This highlights the limitation of COCO and current detectors. Adding SEPC [71] to ATSS [76] decreases all metrics except for AP_L. We found that this reduction does not occur at large test scales in higher USB evaluation protocols (see Supplementary Material). UniverseNet-20.08 shows worse results than UniverseNet in some metrics, probably due to the light use of DCN for fast inference. Table 11 shows the M109s results. Interestingly, improvements by ATSS [76] are smaller than those on COCO and WOD due to the drop of face AP. We conjecture that this phenomenon comes

from the domain differences discussed in Sec. 3.3 and prior work [49], although we should explore it in future work.

ResNet vs. Swin Transformer. Transformer-based backbones have shown promising results recently. We evaluated a representative one: Swin Transformer [43]. Table 8 shows the results with ATSS [76] detectors (see Supplementary Material for hyperparameters). Swin-T [43] shows lower AP than ResNet-50-B [28, 29] on M109s.

Qualitative results. We show some qualitative results of the best detector (UniverseNet-20.08) in Figure 1. Although most detections are accurate, it still suffers from classification error, localization error, and missing detections of tiny vehicles and small manga faces.

4.3. Rethinking COCO with USB Protocols

We classify state-of-the-art methods on COCO test-dev (as of November 14, 2020) by the proposed protocols without compatibility. The results are shown in Table 12. Although state-of-the-art detectors on the COCO benchmark were trained with various settings, the introduced divisions enable us to compare methods in each division. UniverseNet-20.08d achieves the highest AP (51.3%) in the Standard USB 1.0 protocol. Despite 12.5× fewer epochs, the speed-accuracy trade-offs of UniverseNets are comparable to those of EfficientDet [66] (see also Figure 2). With 13-scale TTA, UniverseNet-20.08d achieves the highest AP (54.1%) in the Huge USB 1.0 protocol. Results in higher protocols than USB 1.0 are scattered. If we ignore the difference of hyperparameter optimization, YOLOv4 [5] shows a better speed-accuracy trade-off than EfficientDet [66] in Standard USB 3.x.

Comparisons across different divisions are difficult. Especially, long training is problematic because it can secretly increase AP without decreasing FPS, unlike large test scales. Nevertheless, the EfficientDet [66], YOLOv4 [5], and SpineNet [18] papers compare methods in their tables without specifying the difference in training epochs. The compatibility of the USB training protocols (Sec. 3.5) resolves this disorder. We hope that many papers report results with the protocols for inclusive, healthy, and sustainable development of detectors.

To simulate the compatibility from Standard USB 3.0 to 1.0, we refer to the training log of the EfficientDet author. The AP of EfficientDet-D4 [66] on COCO minival is 43.8% at 23 epoch [64]. Although it could be improved by changing the learning rate schedule, EfficientDet’s inference efficiency is not compatible with training efficiency.

5. Conclusions and Limitations

We introduced USB, a benchmark for universal-scale object detection. To resolve unfair comparisons in existing benchmarks, we established USB training/evaluation protocols. Using the proposed benchmark, we found weaknesses

Acknowledgments. We are grateful to Dr. Hirokatsu Kataoka for helpful comments. We thank all contributors for the datasets and software libraries. The original image of Figure 1 (left) is *satellite office* by Taiyo FUJII (CC BY 2.0).

References

- [1] Robust Vision Challenge 2020. <http://www.robustvision.net/>, Accessed on Nov. 8, 2020. 2
- [2] Waymo Open Dataset 2D detection leaderboard. <https://waymo.com/open/challenges/2d-detection/>, Accessed on June 18, 2020. 4, 15, 16
- [3] Kiyoharu Aizawa, Azuma Fujimoto, Atsushi Otsubo, Toru Ogawa, Yusuke Matsui, Koki Tsubota, and Hikaru Ikuta. Building a manga dataset “Manga109” with annotations for multimedia applications. *IEEE MultiMedia*, 2020. 2, 3, 4, 12, 13
- [4] Khalid Ashraf, Bichen Wu, Forrest N. Iandola, Matthew W. Moskewicz, and Kurt Keutzer. Shallow networks for high-accuracy road object-detection. *arXiv:1606.01561*, 2016. 16
- [5] Alexey Bochkovskiy, Chien-Yao Wang, and Hong-Yuan Mark Liao. YOLOv4: Optimal speed and accuracy of object detection. *arXiv:2004.10934*, 2020. 2, 4, 5, 7, 8, 15
- [6] Navaneeth Bodla, Bharat Singh, Rama Chellappa, and Larry S. Davis. Soft-NMS – improving object detection with one line of code. In *ICCV*, 2017. 16
- [7] Daniel Bolya, Sean Foley, James Hays, and Judy Hoffman. TIDE: A general toolbox for identifying object detection errors. In *ECCV*, 2020. 12
- [8] Zhaowei Cai. *Towards Universal Object Detection*. PhD thesis, UC San Diego, 2019. 2
- [9] Zhaowei Cai and Nuno Vasconcelos. Cascade R-CNN: Delving into high quality object detection. In *CVPR*, 2018. 2, 6, 7, 8, 15, 17
- [10] Nicolas Carion, Francisco Massa, Gabriel Synnaeve, Nicolas Usunier, Alexander Kirillov, and Sergey Zagoruyko. End-to-end object detection with transformers. In *ECCV*, 2020. 2, 4, 5
- [11] Kai Chen, Jiaqi Wang, Jiangmiao Pang, Yuhang Cao, Yu Xiong, Xiaoxiao Li, Shuyang Sun, Wansen Feng, Ziwei Liu, Jiarui Xu, Zheng Zhang, Dazhi Cheng, Chenchen Zhu, Tianheng Cheng, Qijie Zhao, Buyu Li, Xin Lu, Rui Zhu, Yue Wu, Jifeng Dai, Jingdong Wang, Jianping Shi, Wanli Ouyang, Chen Change Loy, and Dahua Lin. MMDetection: Open mmlab detection toolbox and benchmark. *arXiv:1906.07155*, 2019. 2, 4, 5, 6, 12, 13, 14, 15, 16
- [12] Sijia Chen, Yu Wang, Li Huang, Runzhou Ge, Yihan Hu, Zhuangzhuang Ding, and Jie Liao. 2nd place solution for Waymo Open Dataset challenge – 2D object detection. *arXiv:2006.15507*, 2020. 15
- [13] Yihong Chen, Zheng Zhang, Yue Cao, Liwei Wang, Stephen Lin, and Han Hu. RepPoints v2: Verification meets regression for object detection. In *NeurIPS*, 2020. 1, 8
- [14] Cheng Chi, Fangyun Wei, and Han Hu. RelationNet++: Bridging visual representations for object detection via transformer decoder. In *NeurIPS*, 2020. 1, 8
- [15] Jifeng Dai, Haozhi Qi, Yuwen Xiong, Yi Li, Guodong Zhang, Han Hu, and Yichen Wei. Deformable convolutional networks. In *ICCV*, 2017. 2, 6, 12, 14, 16, 17
- [16] Jian Ding, Nan Xue, Gui-Song Xia, Xiang Bai, Wen Yang, Michael Ying Yang, Serge Belongie, Jiebo Luo, Mihai Datcu, Marcello Pelillo, and Liangpei Zhang. Object detection in aerial images: A large-scale benchmark and challenges. *TPAMI*, 2021. 3
- [17] Piotr Dollár, Christian Wojek, Bernt Schiele, and Pietro Perona. Pedestrian detection: An evaluation of the state of the art. *TPAMI*, 2012. 12, 15
- [18] Xianzhi Du, Tsung-Yi Lin, Pengchong Jin, Golnaz Ghiasi, Mingxing Tan, Yin Cui, Quoc V. Le, and Xiaodan Song. SpineNet: Learning scale-permuted backbone for recognition and localization. In *CVPR*, 2020. 2, 4, 7, 8
- [19] Mark Everingham, S. M. Ali Eslami, Luc Van Gool, Christopher K. I. Williams, John Winn, and Andrew Zisserman. The PASCAL Visual Object Classes challenge: A retrospective. *IJCV*, 2015. 1, 2, 3, 5
- [20] Cheng-Yang Fu, Wei Liu, Ananth Ranga, Amrith Tyagi, and Alexander C. Berg. DSSD : Deconvolutional single shot detector. *arXiv:1701.06659*, 2017. 13
- [21] Shang-Hua Gao, Ming-Ming Cheng, Kai Zhao, Xin-Yu Zhang, Ming-Hsuan Yang, and Philip Torr. Res2Net: A new multi-scale backbone architecture. *TPAMI*, 2021. 2, 6, 12, 14, 15, 16, 17
- [22] Andreas Geiger, Philip Lenz, and Raquel Urtasun. Are we ready for autonomous driving? the KITTI vision benchmark suite. In *CVPR*, 2012. 2, 3, 17
- [23] Golnaz Ghiasi, Yin Cui, Aravind Srinivas, Rui Qian, Tsung-Yi Lin, Ekin D. Cubuk, Quoc V. Le, and Barret Zoph. Simple copy-paste is a strong data augmentation method for instance segmentation. In *CVPR*, 2021. 4
- [24] Ross Girshick, Ilija Radosavovic, Georgia Gkioxari, Piotr Dollár, and Kaiming He. Detectron. <https://github.com/facebookresearch/detectron>, 2018. 2, 4, 5, 14
- [25] Priya Goyal, Piotr Dollár, Ross Girshick, Pieter Noordhuis, Lukasz Wesolowski, Aapo Kyrola, Andrew Tulloch, Yangqing Jia, and Kaiming He. Accurate, large minibatch SGD: Training ImageNet in 1 hour. *arXiv:1706.02677*, 2017. 17
- [26] Agrim Gupta, Piotr Dollár, and Ross Girshick. LVIS: A dataset for large vocabulary instance segmentation. In *CVPR*, 2019. 2
- [27] Kaiming He, Ross Girshick, and Piotr Dollár. Rethinking ImageNet pre-training. In *ICCV*, 2019. 4
- [28] Kaiming He, Xiangyu Zhang, Shaoqing Ren, and Jian Sun. Deep residual learning for image recognition. In *CVPR*, 2016. 2, 5, 6, 7, 12, 14
- [29] Tong He, Zhi Zhang, Hang Zhang, Zhongyue Zhang, Junyuan Xie, and Mu Li. Bag of tricks for image classification with convolutional neural networks. In *CVPR*, 2019. 2, 6, 7, 12, 14, 16, 17
- [30] Derek Hoiem, Yodsawalai Chodpathumwan, and Qieyun Dai. Diagnosing error in object detectors. In *ECCV*, 2012. 6, 12, 15

- [31] Jonathan Huang, Vivek Rathod, Chen Sun, Menglong Zhu, Anoop Korattikara, Alireza Fathi, Ian Fischer, Zbigniew Wojna, Yang Song, Sergio Guadarrama, and Kevin Murphy. Speed/accuracy trade-offs for modern convolutional object detectors. In *CVPR*, 2017. 15
- [32] Zehao Huang, Zehui Chen, Qiaofei Li, Hongkai Zhang, and Naiyan Wang. 1st place solutions of Waymo Open Dataset challenge 2020 – 2D object detection track. *arXiv:2008.01365*, 2020. 3, 5, 15, 16
- [33] Naoto Inoue, Ryosuke Furuta, Toshihiko Yamasaki, and Kiyoharu Aizawa. Cross-domain weakly-supervised object detection through progressive domain adaptation. In *CVPR*, 2018. 2, 3, 13
- [34] Kang Kim and Hee Seok Lee. Probabilistic anchor assignment with IoU prediction for object detection. In *ECCV*, 2020. 1, 8
- [35] Alina Kuznetsova, Hassan Rom, Neil Alldrin, Jasper Uijlings, Ivan Krasin, Jordi Pont-Tuset, Shahab Kamali, Stefan Popov, Matteo Mallocci, Alexander Kolesnikov, Tom Duerig, and Vittorio Ferrari. The Open Images Dataset V4: Unified image classification, object detection, and visual relationship detection at scale. *IJCV*, 2020. 2
- [36] Xiang Li, Wenhai Wang, Lijun Wu, Shuo Chen, Xiaolin Hu, Jun Li, Jinhui Tang, and Jian Yang. Generalized Focal Loss: Learning qualified and distributed bounding boxes for dense object detection. In *NeurIPS*, 2020. 1, 2, 6, 7, 8, 14, 15, 16, 17
- [37] Tsung-Yi Lin, Piotr Dollár, et al. COCO API. <https://github.com/cocodataset/cocoapi>, Accessed on Nov. 8, 2020. 5, 6, 13
- [38] Tsung-Yi Lin, Piotr Dollár, Ross Girshick, Kaiming He, Bharath Hariharan, and Serge Belongie. Feature pyramid networks for object detection. In *CVPR*, 2017. 2, 6, 8, 12, 14, 15
- [39] Tsung-Yi Lin, Priya Goyal, Ross Girshick, Kaiming He, and Piotr Dollár. Focal loss for dense object detection. In *ICCV*, 2017. 2, 6, 7, 8, 12, 14, 15
- [40] Tsung-Yi Lin, Michael Maire, Serge Belongie, James Hays, Pietro Perona, Deva Ramanan, Piotr Dollár, and C. Lawrence Zitnick. Microsoft COCO: Common objects in context. In *ECCV*, 2014. 1, 2, 3, 5, 12, 13
- [41] Li Liu, Wanli Ouyang, Xiaogang Wang, Paul Fieguth, Jie Chen, Xinwang Liu, and Matti Pietikäinen. Deep learning for generic object detection: A survey. *IJCV*, 2020. 1, 2
- [42] Wei Liu, Dragomir Anguelov, Dumitru Erhan, Christian Szegedy, Scott Reed, Cheng-Yang Fu, and Alexander C. Berg. SSD: Single shot multibox detector. In *ECCV*, 2016. 2, 5, 12, 15
- [43] Ze Liu, Yutong Lin, Yue Cao, Han Hu, Yixuan Wei, Zheng Zhang, Stephen Lin, and Baining Guo. Swin Transformer: Hierarchical vision transformer using shifted windows. In *ICCV*, 2021. 7, 15
- [44] Ilya Loshchilov and Frank Hutter. Decoupled weight decay regularization. In *ICLR*, 2019. 15
- [45] Yusuke Matsui, Kota Ito, Yuji Aramaki, Azuma Fujimoto, Toru Ogawa, Toshihiko Yamasaki, and Kiyoharu Aizawa. Sketch-based manga retrieval using Manga109 dataset. *Multimedia Tools and Applications*, 2017. 2, 3, 4, 13
- [46] Kevin Musgrave, Serge Belongie, and Ser-Nam Lim. A metric learning reality check. In *ECCV*, 2020. 12
- [47] Lukáš Neumann, Michelle Karg, Shanshan Zhang, Christian Scharfenberger, Eric Piegert, Sarah Mistr, Olga Prokofyeva, Robert Thiel, Andrea Vedaldi, Andrew Zisserman, and Bernt Schiele. NightOwls: A pedestrians at night dataset. In *ACCV*, 2018. 15, 16
- [48] Lukáš Neumann, Yosuke Shinya, and Zhenyu Xu. NightOwls detection challenge. Presentations at CVPR Workshop on Scalability in Autonomous Driving, 2020. 15, 16
- [49] Toru Ogawa, Atsushi Otsubo, Rei Narita, Yusuke Matsui, Toshihiko Yamasaki, and Kiyoharu Aizawa. Object detection for comics using Manga109 annotations. *arXiv:1803.08670*, 2018. 2, 4, 7, 13, 16
- [50] Chao Peng, Tete Xiao, Zeming Li, Yuning Jiang, Xiangyu Zhang, Kai Jia, Gang Yu, and Jian Sun. MegDet: A large mini-batch object detector. In *CVPR*, 2018. 6, 14, 16, 17
- [51] Siyuan Qiao, Liang-Chieh Chen, and Alan Yuille. DetectorRS: Detecting objects with recursive feature pyramid and switchable atrous convolution. *arXiv:2006.02334*, 2020. 2, 8
- [52] Joseph Redmon, Santosh Divvala, Ross Girshick, and Ali Farhadi. You Only Look Once: Unified, real-time object detection. In *CVPR*, 2016. 2
- [53] Shaoqing Ren, Kaiming He, Ross Girshick, and Jian Sun. Faster R-CNN: Towards real-time object detection with region proposal networks. In *NIPS*, 2015. 2, 6, 7, 8, 12, 15
- [54] Henry A. Rowley, Shumeet Baluja, and Takeo Kanade. Neural network-based face detection. *TPAMI*, 1998. 2, 12
- [55] Olga Russakovsky, Jia Deng, Hao Su, Jonathan Krause, Sanjeev Satheesh, Sean Ma, Zhiheng Huang, Andrej Karpathy, Aditya Khosla, Michael S. Bernstein, Alexander C. Berg, and Li Fei-Fei. ImageNet Large Scale Visual Recognition Challenge. *IJCV*, 2015. 1, 5, 6, 12, 15
- [56] Roy Schwartz, Jesse Dodge, Noah A. Smith, and Oren Etzioni. Green AI. *Communications of the ACM*, 2020. 2, 4, 12
- [57] Shuai Shao, Zeming Li, Tianyuan Zhang, Chao Peng, Gang Yu, Xiangyu Zhang, Jing Li, and Jian Sun. Objects365: A large-scale, high-quality dataset for object detection. In *ICCV*, 2019. 2
- [58] Yosuke Shinya, Edgar Simo-Serra, and Taiji Suzuki. Understanding the effects of pre-training for object detectors via eigenspectrum. In *ICCV Workshop on Neural Architects*, 2019. 5, 14
- [59] Bharat Singh and Larry S. Davis. An analysis of scale invariance in object detection – SNIP. In *CVPR*, 2018. 2, 3, 12
- [60] Guanglu Song, Yu Liu, and Xiaogang Wang. Revisiting the sibling head in object detector. In *CVPR*, 2020. 8
- [61] Pei Sun, Henrik Kretzschmar, Xerxes Dotiwalla, Aurelien Chouard, Vijaysai Patnaik, Paul Tsui, James Guo, Yin Zhou, Yuning Chai, Benjamin Caine, Vijay Vasudevan, Wei Han, Jiquan Ngiam, Hang Zhao, Aleksei Timofeev, Scott Etinger, Maxim Krivokon, Amy Gao, Aditya Joshi, Yu Zhang, Jonathon Shlens, Zhifeng Chen, and Dragomir Anguelov.

- Scalability in perception for autonomous driving: Waymo Open Dataset. In *CVPR*, 2020. 2, 3, 4, 5, 12, 13, 16, 17
- [62] Christian Szegedy, Wei Liu, Yangqing Jia, Pierre Sermanet, Scott Reed, Dragomir Anguelov, Dumitru Erhan, Vincent Vanhoucke, and Andrew Rabinovich. Going deeper with convolutions. In *CVPR*, 2015. 2, 12
- [63] Christian Szegedy, Vincent Vanhoucke, Sergey Ioffe, Jon Shlens, and Zbigniew Wojna. Rethinking the inception architecture for computer vision. In *CVPR*, 2016. 12
- [64] Mingxing Tan. A comment about the training log of EfficientDet. <https://github.com/google/automl/issues/380#issuecomment-800814557>, Accessed on Aug. 23, 2021. 7
- [65] Mingxing Tan and Quoc V. Le. EfficientNet: Rethinking model scaling for convolutional neural networks. In *ICML*, 2019. 15
- [66] Mingxing Tan, Ruoming Pang, and Quoc V. Le. EfficientDet: Scalable and efficient object detection. In *CVPR*, 2020. 2, 4, 5, 7, 8, 12
- [67] Mingxing Tan, Ruoming Pang, and Quoc V. Le. EfficientDet: Scalable and efficient object detection. *arXiv:1911.09070v7*, 2020. 2, 4, 5, 8
- [68] Zhi Tian, Chunhua Shen, Hao Chen, and Tong He. FCOS: Fully convolutional one-stage object detection. In *ICCV*, 2019. 2, 8
- [69] Angelina Wang, Arvind Narayanan, and Olga Russakovsky. REVISE: A tool for measuring and mitigating bias in visual datasets. In *ECCV*, 2020. 12
- [70] Xudong Wang, Zhaowei Cai, Dashan Gao, and Nuno Vasconcelos. Towards universal object detection by domain attention. In *CVPR*, 2019. 1, 3, 5, 13
- [71] Xinjiang Wang, Shilong Zhang, Zhuoran Yu, Litong Feng, and Wayne Zhang. Scale-equalizing pyramid convolution for object detection. In *CVPR*, 2020. 1, 2, 6, 7, 8, 12, 14, 16, 17
- [72] Saining Xie, Ross Girshick, Piotr Dollár, Zhuowen Tu, and Kaiming He. Aggregated residual transformations for deep neural networks. In *CVPR*, 2017. 8
- [73] Hang Xu, Chenhan Jiang, Dapeng Feng, Chaoqiang Ye, Rui Sun, and Xiaodan Liang. SPNAS-Noah: Single Cascade-RCNN with backbone architecture adaption for Waymo 2D detection. <https://sites.google.com/view/cvpr20-scalability/wod-reports>, Accessed on June 21, 2020. 15
- [74] Shuo Yang, Ping Luo, Chen-Change Loy, and Xiaoou Tang. WIDER FACE: A face detection benchmark. In *CVPR*, 2016. 2
- [75] Xuehui Yu, Yuqi Gong, Nan Jiang, Qixiang Ye, and Zhenjun Han. Scale match for tiny person detection. In *WACV*, 2020. 2, 3, 12, 15
- [76] Shifeng Zhang, Cheng Chi, Yongqiang Yao, Zhen Lei, and Stan Z. Li. Bridging the gap between anchor-based and anchor-free detection via adaptive training sample selection. In *CVPR*, 2020. 1, 2, 6, 7, 8, 12, 14, 15, 16

Supplementary Material

A. Discussions on Research Ethics

Potential negative societal impacts. Improving the accuracy and universality of object detectors could improve the performance of autonomous weapons. To mitigate the risk, we could develop more detectors for entertainment to increase people’s happiness and decrease their hatred. Besides, detectors might be misused for surveillance systems (*e.g.*, as a part of person tracking methods). To mitigate the risk, the computer vision community will need to have discussions with national and international organizations to regulate them appropriately.

Existing assets. We used the assets listed in Table 13. See our codes for more details. Refer to the papers [3, 40, 61] and the URLs for how the datasets were collected.

Consent. See [3] for M109s. For the other datasets, we could not find whether and how consent was obtained. It will be impossible to obtain consent from people recorded in datasets for autonomous driving such as WOD [61].

Privacy. Faces and license plates in WOD [61] are blurred. COCO images may harm privacy because they probably contain personally identifiable information. However, COCO [40] is so popular that the computer vision community cannot stop using it suddenly. This paper will be a step toward reducing the dependence on COCO.

Offensive contents. M109s covers various contents [3]. This characteristic is useful to develop universal-scale object detectors. One of the authors checked many images of the three datasets with eyes and felt that some images in M109s may be considered offensive (*e.g.*, violence in battle manga and nudity in romantic comedy). Thus, researchers should be careful how they use it. It is also valuable to develop methods to detect such scenes using the dataset.

Compute. Considering the numbers of training images, training for USB takes about $1.7 (\approx \frac{118287+79735+6467}{118287})$ times longer than that for COCO. This is reasonable as a next-generation benchmark after COCO. Furthermore, the proposed protocols provide incentives to avoid computationally intensive settings [66].

B. Details of Related Work

B.1. Components for Multi-Scale Object Detection

Backbones and modules. Inception module [62] arranges 1×1 , 3×3 , and 5×5 convolutions to cover multi-scale regions. Residual block [28] adds multi-scale features from shortcut connections and 3×3 convolutions. ResNet-C and ResNet-D [29] replace the first layer of ResNet with the deep stem (three 3×3 convolutions) [63]. Res2Net module [21] stacks 3×3 convolutions hierarchically to represent multi-scale features. Res2Net-v1b [21] adopts deep stem with Res2Net module. Deformable convolution module in

Deformable Convolutional Networks (DCN) [15] adjusts receptive field adaptively by deforming the sampling locations of standard convolutions. These modules are mainly used in backbones.

Necks. To combine and enhance backbones’ representation, necks follow backbones. Feature Pyramid Networks (FPN) [38] adopt top-down path and lateral connections like architectures for semantic segmentation. Scale-Equalizing Pyramid Convolution (SEPC) [71] introduces pyramid convolution across feature maps with different resolutions and utilizes DCN to align the features.

Heads and training sample selection. Faster R-CNN [53] spreads multi-scale anchors over a feature map. SSD [42] spreads multi-scale anchors over multiple feature maps with different resolutions. Adaptive Training Sample Selection (ATSS) [76] eliminates the need for multi-scale anchors by dividing positive and negative samples according to object statistics across pyramid levels.

Multi-scale training and testing. Traditionally, the image pyramid is an essential technique to handle multi-scale objects [54]. Although recent detectors can output multi-scale objects from a single-scale input, many studies use multi-scale inputs to improve performance [39, 53, 71, 76]. In a popular implementation [11], multi-scale training randomly chooses a scale at each iteration for (training-time) data augmentation. Multi-scale testing infers multi-scale inputs and merges their outputs for Test-Time Augmentation (TTA). Scale Normalization for Image Pyramids (SNIP) [59] limits the range of object scales at each image scale during training and testing.

B.2. Scale-Wise Metrics

Many studies have introduced different scale-wise metrics [7, 17, 30, 40, 55, 69, 75]. Unlike these studies, we introduce two types of finer scale-wise metrics based on the absolute scale and relative scale [75]. More importantly, we evaluated them on the datasets that have extensive scale variations and many instances in multiple domains.

B.3. Criticism of Experimental Settings

For fair, inclusive, and efficient research, many previous studies have criticized experimental settings (*e.g.*, [46, 56]). These previous studies do not propose fair and practical protocols for object detection benchmarks.

C. Details of Protocols

C.1. Dataset Splits of Manga109-s

The *Manga109-s* dataset (87 volumes) is a subset of the full *Manga109* dataset (109 volumes) [3]. Unlike the full *Manga109* dataset, the *Manga109-s* dataset can be used by commercial organizations. The dataset splits for the full

Asset	Version	URL	License
COCO [40]	2017	https://cocodataset.org/	Annotations: CC-BY 4.0; images: various licenses
WOD [61]	1.2	https://waymo.com/open/	Custom license
Manga109-s [3, 45]	2020.12.18	http://www.manga109.org/	Custom license
COCO API [37]	2.0	https://github.com/cocodataset/cocoapi	2-Clause BSD License
WOD (code)	—	https://github.com/waymo-research/waymo-open-dataset	Apache License 2.0
Manga109 API	0.3.1	https://github.com/manga109/manga109api	MIT License
MMDetection [11]	2.17.0	https://github.com/open-mmlab/mmdetection	Apache License 2.0

Table 13. Existing assets we used.

Volume	Genre
<i>15test set:</i>	
Aku-Ham	Four-frame cartoons
Bakuretsu! Kung Fu Girl	Romantic comedy
Doll Gun	Battle
Eva Lady	Science fiction
Hinagiku Kenzan!	Love romance
Kyokugen Cyclone	Sports
Love Hina vol. 1	Romantic comedy
Momoyama Haikagura	Historical drama
Tennen Senshi G	Humor
Uchi no Nyan's Diary	Animal
Unbalance Tokyo	Science fiction
Yamato no Hane	Sports
Youma Kourin	Fantasy
Yume no Kayoiji	Fantasy
Yumeiro Cooking	Love romance
<i>4val set:</i>	
Healing Planet	Science fiction
Love Hina vol. 14	Romantic comedy
Seijinki Vulnus	Battle
That's! Izumiko	Fantasy
<i>68train set: All the other volumes</i>	

Table 14. Manga109-s dataset splits (87 volumes in total).

Manga109 dataset used in prior work [49] cannot be used for the Manga109-s dataset.

We defined the Manga109-s dataset splits shown in Table 14. Unlike alphabetical order splits used in the prior work [49], we selected the volumes carefully. The `15test` set was selected to be well-balanced for reliable evaluation. Five volumes in the `15test` set were selected from the 10 test volumes used in [49] to enable partially direct comparison. All the authors of the `15test` and `4val` set are different from those of the `68train` set to evaluate generalizability.

C.2. Number of Images

There are 118,287 images in COCO `train2017`, 5,000 in COCO `val2017`, 79,735 in WOD `f0train`, 20,190 in WOD `f0val`, 6,467 in M109s `68train`, 399 in M109s `4val`, and 1,289 in M109s `15test`. Following prior work [49], we exclude M109s images without annotations because objects in irregular pages are not annotated.

C.3. Importance of Many Instances

Here, we highlight the importance of a larger number of instances than UODB [70]. We show that if we introduced scale-wise metrics to UODB, the results would be unreliable. Watercolor2k, one of the datasets adopted by UODB,

has 6 classes and 27 bicycle instances [33]. If we equally divided the dataset for training and evaluation and they had the same number of small, medium, and large bicycles, the average number of bicycles of a particular scale in the evaluation split would be 4.5. Since the 4.5 bicycles affect $\frac{1}{6}$ of a scale-wise metric, a single error can change the results by 3.7%. Thus, randomness can easily reverse the ranking between methods, making the benchmark results unreliable.

C.4. Exceptions of Protocols

The rounding error of epochs between epoch- and iteration-based training can be ignored when calculating the maximum epochs. Small differences of eight pixels or less can be ignored when calculating the maximum resolutions. For example, DSSD513 [20] will be compared in Mini USB.

C.5. Constraints on Training Time

We do not adopt constraints on training time as the major constraints of the training protocols because they have the following issues.

- It is difficult to measure training time on unified hardware.
- It is complicated to measure training time, calculate allowable epochs, and set learning rate schedules for each model.
- It is difficult to compare with previous studies, which align the number of epochs.
- They will reduce the value of huge existing resources for standard training epochs (trained models, configuration files, and experimental results) provided by popular object detection libraries such as MMDetection [11].
- They overemphasize implementation optimization rather than trial and error of novel methods.
- There are overlaps between the factors of training time and those of inference time.

The proposed constraints on training epochs are much easier to adopt and more reasonable. Furthermore, our protocols compensate for the shortcomings of the training epoch constraints by defining the provisions for hyperparameter optimization and data augmentation.

Method	Head		Neck			Backbone			Input	FPS	COCO (1× schedule)					
	ATSS	GFL	PConv	DCN	iBN	Res2	DCN	SyncBN	MStrain		AP	AP ₅₀	AP ₇₅	AP _S	AP _M	AP _L
RetinaNet [39]										33.9	36.5	55.4	39.1	20.4	40.3	48.1
ATSS [76]	✓									35.2	39.4	57.6	42.8	23.6	42.9	50.3
GFL [36]	✓	✓								37.2	40.2	58.4	43.3	23.3	44.0	52.2
ATSEPC [71, 76]	✓		✓		P, LC					25.0	42.1	59.9	45.5	24.6	46.1	55.0
UniverseNet	✓				P, LC	✓	c3-c5		✓	17.3	46.7	65.0	50.7	29.2	50.6	61.4
UniverseNet+GFL	✓	✓	✓		P, LC	✓	c3-c5		✓	17.5	47.5	65.8	51.8	29.2	51.6	62.5
UniverseNet-20.08d	✓	✓	✓		P, LC	✓	c3-c5	✓	✓	17.3	48.6	67.1	52.7	30.1	53.0	63.8
UniverseNet-20.08	✓	✓	✓		LC	✓	c5	✓	✓	24.9	47.5	66.0	51.9	28.9	52.1	61.9
UniverseNet-20.08 w/o SEPC [71]	✓	✓				✓	c5	✓	✓	26.7	45.8	64.6	50.0	27.6	50.4	59.7
UniverseNet-20.08 w/o Res2Net-v1b [21]	✓	✓	✓		LC	✓	c5	✓	✓	32.8	44.7	62.8	48.4	27.1	48.8	59.5
UniverseNet-20.08 w/o DCN [15]	✓	✓	✓			✓	c5	✓	✓	27.8	45.9	64.5	49.8	28.9	49.9	59.0
UniverseNet-20.08 w/o iBN, SyncBN [50, 71]	✓	✓	✓		LC	✓	c5	✓	✓	25.7	45.8	64.0	50.2	27.9	50.0	59.8
UniverseNet-20.08 w/o MStrain	✓	✓	✓		LC	✓	c5	✓	✓	24.8	45.9	64.5	49.6	27.4	50.5	60.1

Table 15. Architectures of UniverseNets with a summary of ablation studies on COCO *minival*. See Sec. E.6 for step-by-step improvements. All results are based on MMDetection [11] v2. The “Head” methods (ATSS and GFL) affect losses and training sample selection. Res2: Res2Net-v1b [21]. PConv (Pyramid Convolution) and iBN (integrated Batch Normalization) are the components of SEPC [71]. The DCN columns indicate where to apply DCN. “P”: The PConv modules in the combined head of SEPC [71]. “LC”: The extra head of SEPC for localization and classification [71]. “c3-c5”: conv3_x, conv4_x, and conv5_x layers in ResNet-style backbones [28]. “c5”: conv5_x layers in ResNet-style backbones [28]. ATSEPC: ATSS with SEPC (without iBN). MStrain: Multi-scale training. FPS: Frames per second on one V100 with mixed precision.

C.6. Characteristics of Scale-Wise Metrics

ASAP and COCO-style scale-wise metrics are based on the absolute scale. It has a weakness that it changes with image resizing. To limit inference time and GPU memory consumption, and to ensure fair comparisons, input image scales are typically resized. If they are smaller than the original image scales, relative scales have direct effects on accuracy rather than absolute scales. Furthermore, objects with the same absolute scale in the original images may have different absolute scales in the input images. Fluctuating object scale thresholds is not desirable for scale-wise metrics.

In addition, ASAP is not suitable for evaluating accuracy for very large objects. It may be impossible to calculate ASAP for large absolute scales on some datasets. In the case of USB, we cannot calculate $ASAP_{\infty}$ on COCO because the absolute scales of COCO objects are smaller than 1024 (we filled $ASAP_{\infty}$ on COCO with zero in experiments). Furthermore, ASAP for large absolute scales may show unusual behavior. For example, in the evaluation of $ASAP_{\infty}$ on M109s, all predictions larger than 1024 of absolute scales have larger IoUs than 0.5 with an object of image resolution size (1654×1170).

We prefer RSAP to ASAP due to the above-mentioned weaknesses of ASAP. Absolute scales may be important depending on whether and how participants resize images. In that case, RSAP and ASAP can be used complementarily.

D. Details of UniverseNets

For fast and accurate detectors for USOD, we designed UniverseNets. We adopted single-stage detectors for efficiency. We show the detailed architectures in Table 15.

As a baseline model, we used the RetinaNet [39] implemented in MMDetection [11]. Specifically, the backbone is

ResNet-50-B [29] (a variant of ResNet-50 [28], also known as the PyTorch style). The neck is FPN [38]. We used focal loss [39], single-scale training, and single-scale testing.

Built on the RetinaNet baseline, we designed *UniverseNet* by collecting human wisdom about multi-scale object detection as of May 2020. We used ATSS [76] and SEPC without iBN [71] (hereafter referred to as *ATSEPC*). The backbone is Res2Net-50-v1b [21]. We adopted Deformable Convolutional Networks (DCN) [15] in the backbone and neck. We used multi-scale training. Unless otherwise stated, we used single-scale testing for efficiency.

By adding GFL [36], SyncBN [50], and iBN [71], we designed three variants of UniverseNet around August 2020. *UniverseNet-20.08d* heavily uses DCN [15]. *UniverseNet-20.08* speeds up inference (and training) by the light use of DCN [15, 71]. *UniverseNet-20.08s* further speeds up inference using the ResNet-50-C [29] backbone.

E. Details of Experiments

Here, we show the details of experimental settings and results. See also the code to reproduce our settings including minor hyperparameters.

E.1. Common Settings

We follow the learning rate schedules of MMDetection [11], which are similar to those of Detectron [24]. Specifically, the learning rates are reduced by 10× in two predefined epochs. Epochs for the first learning rate decay, the second decay, and ending training are (8, 11, 12) for the 1× schedule, (16, 22, 24) for the 2× schedule, and (16, 19, 20) for the 20e schedule. To avoid overfitting by small learning rates [58], the 20e schedule is reasonable. We mainly used the 1× schedule (12 epochs). For comparison with state-of-the-art methods on COCO, we used

the $2\times$ schedule (24 epochs) for most models and the 20x schedule (20 epochs) for UniverseNet-20.08d due to overfitting with the $2\times$ schedule. For comparison with state-of-the-art methods on WOD, we trained UniverseNet on the WOD full training set for 7 epochs. We used a learning rate of 10^{-3} for 6 epochs and 10^{-4} for the last epoch.

We mainly used ImageNet [55] pre-trained backbones that are standard in MMDetection [11]. Some pre-trained Res2Net backbones not supported in MMDetection were downloaded from the Res2Net [21] repository. We used the COCO pre-trained models of the MMDetection [11] repository for existing methods (Faster R-CNN [53] with FPN [38], Cascade R-CNN [9], RetinaNet [39], ATSS [76], and GFL [36]). We trained most models with mixed precision and 4 GPUs ($\times 4$ images per GPU). We mainly used NVIDIA T4 GPUs on the Google Cloud Platform. All results on USB and all results of UniverseNets are single model results without ensemble. We excluded images without annotations during training. We could not train each object detector multiple times with different random seeds to report error bars because training object detectors is too computationally expensive.

For training ATSS [76] with Swin Transformer [43], we follow the optimizer settings of the Swin paper [43]. Specifically, we used the AdamW optimizer [44] with an initial learning rate of 10^{-4} and a weight decay of 0.05. For M109s, we used an initial learning rate of 4×10^{-4} , roughly tuned from choices $\{2\times 10^{-4}, 4\times 10^{-4}, 8\times 10^{-4}\}$.

E.2. Settings on COCO

For comparison with state-of-the-art methods with TTA on COCO, we used soft voting with 13-scale testing and horizontal flipping following the original implementation of ATSS [76]. Specifically, shorter side pixels are (400, 500, 600, 640, 700, 800, 900, 1000, 1100, 1200, 1300, 1400, 1800), while longer side pixels are their $1.667\times$. For the 13 test scales, target objects are limited to corresponding 13 predefined ranges ((96, ∞), (96, ∞), (64, ∞), (64, ∞), (64, ∞), (0, ∞), (0, ∞), (0, ∞), (0, 256), (0, 256), (0, 192), (0, 192), (0, 96)), where each tuple denotes the minimum and maximum absolute scales. We also evaluated 5-scale TTA because the above-mentioned ATSS-style TTA is slow. We picked (400, 600, 800, 1000, 1200) for shorter side pixels, and ((96, ∞), (64, ∞), (0, ∞), (0, ∞), (0, 256)) for absolute scale ranges.

E.3. Settings on NightOwls

NightOwls [47] is a dataset for person detection at night. It contains three categories (pedestrian, bicycle driver, and motorbike driver). In contrast to WOD, it is important to detect medium or large objects because the evaluation of NightOwls follows the *reasonable* setting [17] where small objects (less than 50 pixels tall) are ignored. We prevented

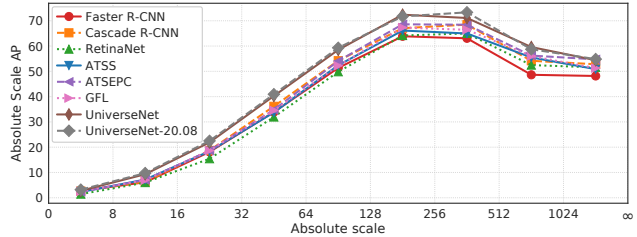


Figure 6. Absolute Scale AP on USB.

Rank	Method	# Models		AP/L2
		Multi-stage	Single-stage	
<i>Methods including multi-stage detector:</i>				
1	RW-TSDet [32]	6+		74.43
2	HorizonDet [12]	4	8	70.28
3	SPNAS-Noah [73]	2		69.43
<i>Single-stage detectors:</i>				
7	UniverseNet (Ours)		1	67.42
13	YOLO V4 [5]		1+	58.08
14	ATSS-Efficientnet [65, 76]		1+	56.99

Table 16. Waymo Open Dataset Challenge 2020 2D detection [2].

Rank	Method	Test scale	Test flip	MR
1	UniverseNet	1280 \times 800, 1536 \times 960	✓	5.67
–	UniverseNet	1280 \times 800		7.49
2	DeepBlueAI [48]	1920 \times 1280, 2048 \times 1280	✓	8.06
3	dereyly [48]	—	—	10.29

Table 17. NightOwls Detection Challenge 2020 all objects track. MR: Average Miss Rate (%) on `test` set (*reasonable* setting).

the overfitting of the driver categories (bicycle driver and motorbike driver) in two ways. The first is to map the classifier layer of a WOD pre-trained model. We transferred the weights for cyclists learned on the richer WOD to those for the NightOwls driver categories. The second is early stopping. We trained the model for 2 epochs (4,554 iterations) without background images.

E.4. Evaluation with Scale-Wise Metrics

We show RSAP and ASAP on USB in Figures 4 and 6, respectively. They do not increase monotonically but rather decrease at relative scales greater than $1/4$ or absolute scales greater than 512. The difficulty of very large objects may be caused by truncation or unusual viewpoints [30]. Except for the issues of $ASAP_{\infty}$ discussed in Sec. C.6, ASAP shows similar changes to RSAP. We conjecture that this is because image resolutions do not change much in each dataset of USB. $RSAP_{\frac{1}{64}}$ and $ASAP_{16}$ are less than 10%, which indicates the difficulty of tiny object detection [75]. RetinaNet [39] shows low AP for small objects, while Faster R-CNN [53] with FPN [38] shows low AP for large objects. These results are consistent with the benchmark results of previous work [31], which compares SSD [42] with Faster R-CNN without FPN on COCO. For further analysis, it will be worth comparing the design choice of pyramid levels [39, 75].

Method	AP	AP ₅₀	AP ₇₅	AP _S	AP _M	AP _L
ATSS [76]	39.4	57.6	42.8	23.6	42.9	50.3
ATSEPC [71,76]	42.1	59.9	45.5	24.6	46.1	55.0

(a) AP improvements by SEPC without iBN [71].

Method	AP	AP ₅₀	AP ₇₅	AP _S	AP _M	AP _L
ATSEPC [71,76]	42.1	59.9	45.5	24.6	46.1	55.0
UniverseNet	46.7	65.0	50.7	29.2	50.6	61.4

(b) AP improvements by Res2Net-v1b [21], DCN [15], and multi-scale training.

Method	AP	AP ₅₀	AP ₇₅	AP _S	AP _M	AP _L
UniverseNet	46.7	65.0	50.7	29.2	50.6	61.4
UniverseNet+GFL	47.5	65.8	51.8	29.2	51.6	62.5

(c) AP improvements by GFL [36].

Method	AP	AP ₅₀	AP ₇₅	AP _S	AP _M	AP _L
UniverseNet+GFL	47.5	65.8	51.8	29.2	51.6	62.5
UniverseNet-20.08d	48.6	67.1	52.7	30.1	53.0	63.8

(d) AP improvements by SyncBN [50] and iBN [71].

Method	DCN	FPS	AP	AP ₅₀	AP ₇₅	AP _S	AP _M	AP _L
UniverseNet-20.08d	heavy	17.3	48.6	67.1	52.7	30.1	53.0	63.8
UniverseNet-20.08	light	24.9	47.5	66.0	51.9	28.9	52.1	61.9

(e) Speeding up by the light use of DCN [15,71].

Method	FPS	AP	AP ₅₀	AP ₇₅	AP _S	AP _M	AP _L
UniverseNet-20.08	24.9	47.5	66.0	51.9	28.9	52.1	61.9
w/o SEPC [71]	26.7	45.8	64.6	50.0	27.6	50.4	59.7
w/o Res2Net-v1b [21]	32.8	44.7	62.8	48.4	27.1	48.8	59.5
w/o DCN [15]	27.8	45.9	64.5	49.8	28.9	49.9	59.0
w/o multi-scale training	24.8	45.9	64.5	49.6	27.4	50.5	60.1
w/o SyncBN, iBN [50,71]	25.7	45.8	64.0	50.2	27.9	50.0	59.8

(f) Ablation from UniverseNet-20.08. Replacing Res2Net-v1b backbone with ResNet-B [29] has the largest effects.

Backbone	FPS	AP	AP ₅₀	AP ₇₅	AP _S	AP _M	AP _L
ResNet-50-B [29]	32.8	44.7	62.8	48.4	27.1	48.8	59.5
ResNet-50-C [29]	32.4	45.8	64.2	50.0	28.8	50.1	60.0
Res2Net-50 [21]	25.0	46.3	64.7	50.3	28.2	50.6	60.8
Res2Net-50-v1b [21]	24.9	47.5	66.0	51.9	28.9	52.1	61.9

(g) UniverseNet-20.08 with different backbones.

Table 18. Ablation studies on COCO minival.

E.5. Comparison with State-of-the-Art

WOD. For comparison with state-of-the-art methods on WOD, we submitted the detection results of UniverseNet to the Waymo Open Dataset Challenge 2020 2D detection, a competition held at a CVPR 2020 workshop. The primary metric is AP/L2, a KITTI-style AP evaluated with LEVEL_2 objects [2, 61]. We used multi-scale testing with soft-NMS [6]. The shorter side pixels of test scales are (960, 1600, 2240), including 8 pixels padding. These scales enable utilizing SEPC [71] (see Sec. E.7) and detecting small objects. Table 16 shows the top teams’ results. UniverseNet achieves 67.42% AP/L2 without multi-stage detectors, ensembles, expert models, or heavy backbones, unlike other top methods. RW-TSDet [32] overwhelms other multi-stage detectors, whereas UniverseNet overwhelms other single-stage detectors. These two methods used light backbones and large test scales [4]. Interestingly, the maximum test scales are the same (3360×2240). We conjecture that this is not a coincidence but a convergence caused by searching the accuracy saturation point.

Manga109-s. To the best of our knowledge, no prior work has reported detection results on the *Manga109-s* dataset (87 volumes). Although many settings differ, the state-of-the-art method on the full *Manga109* dataset (109 volumes, non-public to commercial organizations) achieves 77.1–92.0% (mean: 84.2%) AP₅₀ on ten test volumes [49]. The mean AP₅₀ of UniverseNet-20.08 on the 15_{test} set (92.5%) is higher than those results.

NightOwls. To evaluate the generalization ability, we show the results on another dataset out of USB. We trained UniverseNet on the NightOwls [47], a dataset for person detection at night, from the WOD pre-trained model in Sec. E.5. The top teams’ results of the NightOwls Detection Chal-

lenge 2020 are shown in Table 17. UniverseNet is more accurate than other methods, even without TTA, and should be faster than the runner-up method that uses larger test scales and a heavy model (Cascade R-CNN, ResNeXt-101, CB-Net, Double-Head, DCN, and soft-NMS) [48].

E.6. Ablation Studies for UniverseNets

We show the results of ablation studies for UniverseNets on COCO in Table 18. As shown in Table 18a, ATSEPC (ATSS [76] with SEPC without iBN [71]) outperforms ATSS by a large margin. The effectiveness of SEPC for ATSS is consistent with those for other detectors reported in the SEPC paper [71]. As shown in Table 18b, UniverseNet further improves AP metrics by ~5% by adopting Res2Net-v1b [21], DCN [15], and multi-scale training. As shown in Table 18c, adopting GFL [36] improves AP by 0.8%. There is room for improvement of AP_S in the Quality Focal Loss of GFL [36]. As shown in Table 18d, UniverseNet-20.08d achieves 48.6% AP by making more use of BatchNorm (SyncBN [50] and iBN [71]). It is much more accurate than other models trained for 12 epochs using ResNet-50-level backbones (e.g., ATSS: 39.4% [11,76], GFL: 40.2% [11,36]). On the other hand, the inference is not so fast (less than 20 FPS) due to the heavy use of DCN [15]. UniverseNet-20.08 speeds up inference by the light use of DCN [15,71]. As shown in Table 18e, UniverseNet-20.08 is 1.4× faster than UniverseNet-20.08d at the cost of a ~1% AP drop. To further verify the effectiveness of each technique, we conducted ablation from UniverseNet-20.08 shown in Table 18f. All techniques contribute to the high AP of UniverseNet-20.08. Ablating the Res2Net-v1b backbone (replacing Res2Net-50-v1b [21] with ResNet-50-B [29]) has the largest effects. Res2Net-

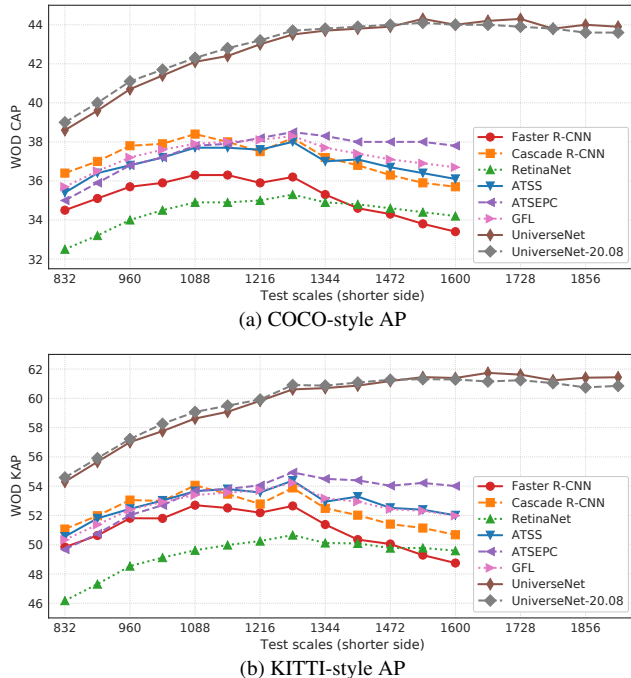


Figure 7. Test scales vs. different AP metrics on WOD f_{0val} .

v1b improves AP by 2.8% and increases the inference time by $1.3\times$. To further investigate the effectiveness of backbones, we trained variants of UniverseNet-20.08 as shown in Table 18g. Although the Res2Net module [21] makes inference slower, the deep stem used in ResNet-50-C [29] and Res2Net-50-v1b [21] improves AP metrics with similar speeds. UniverseNet-20.08s (the variant using the ResNet-50-C backbone) shows a good speed-accuracy trade-off by achieving 45.8% AP and over 30 FPS.

E.7. Effects of Test Scales

We show the results on WOD at different test scales in Figure 7a. Single-stage detectors require larger test scales than multi-stage detectors to achieve peak performance, probably because they cannot extract features from precisely localized region proposals. Although ATSEPC shows lower AP than ATSS at the default test scale (1248×832 in Standard USB), it outperforms ATSS at larger test scales (e.g., 1920×1280 in Large USB). We conjecture that we should enlarge object scales in images to utilize SEPC [71] because its DCN [15] enlarges effective receptive fields. SEPC and DCN prefer large objects empirically (Tables 18a, 18f, [15, 71]), and DCN [15] cannot increase the sampling points for objects smaller than the kernel size in principle. By utilizing the characteristics of SEPC and multi-scale training, UniverseNets achieve the highest AP in a wide range of test scales.

Pre-training	AP	AP ₅₀	AP ₇₅	AP _S	AP _M	AP _L	body	face	frame	text
ImageNet	68.9	92.2	73.3	19.9	42.6	75.8	64.3	47.6	93.0	70.7
COCO 1 \times	69.9	92.5	74.3	20.5	43.6	77.1	66.6	48.0	93.7	71.2
COCO 2 \times	69.8	92.3	74.0	20.5	43.4	77.0	66.5	47.8	93.8	71.2

Table 19. UniverseNet-20.08 on Manga109-s 15test with different pre-trained models.

E.8. Evaluation with KITTI-Style AP

We evaluated the KITTI-style AP (KAP) on WOD. KAP is a metric used in benchmarks for autonomous driving [22, 61]. Using different IoU thresholds (0.7 for vehicles, and 0.5 for pedestrians and cyclists), KAP is calculated as $KAP = (AP_{0.7,veh.} + AP_{0.5,ped.} + AP_{0.5,cyc.})/3$. The results of KAP are shown in Figure 7b. GFL [36] and Cascade R-CNN [9], which focus on localization quality, are less effective for KAP.

E.9. Effects of COCO Pre-Training

To verify the effects of COCO pre-training, we trained UniverseNet-20.08 on M109s from different pre-trained models. Table 19 shows the results. COCO pre-training improves all the metrics, especially body AP.

We also trained models with the eight methods on M109s from ImageNet pre-trained backbones. We halved the learning rates in Table 6 and doubled warmup iterations [25] (from 500 to 1,000) because the training of single-stage detectors without COCO pre-training or SyncBN [50] is unstable. The CAP without COCO pre-training is 1.9% lower than that with COCO pre-training (Table 7) on average.